Little Ice Age cold interval in West Antarctica: Evidence from borehole temperature at the West Antarctic Ice Sheet (WAIS) Divide

Anais J. Orsi,[1] Bruce D. Cornuelle,[1] and Jeffrey P. Severinghaus[1]

[1]   The largest climate anomaly of the last 1000 years in the Northern Hemisphere was the Little Ice Age (LIA) from 1400–1850 C.E., but little is known about the signature of this event in the Southern Hemisphere, especially in Antarctica. We present temperature data from a 300 m borehole at the West Antarctic Ice Sheet (WAIS) Divide. Results show that WAIS Divide was colder than the last 1000-year average from 1300 to 1800 C.E. The temperature in the time period 1400–1800 C.E. was on average 0.52 ± 0.28°C colder than the last 100-year average. This amplitude is about half of that seen at Greenland Summit (GRIP). This result is consistent with the idea that the LIA was a global event, probably caused by a change in solar and volcanic forcing, and was not simply a seesaw-type redistribution of heat between the hemispheres as would be predicted by some ocean-circulation hypotheses. The difference in the magnitude of the LIA between Greenland and West Antarctica suggests that the feedbacks amplifying the radiative forcing may not operate in the same way in both regions. **Citation:** Orsi, A. J., B. D. Cornuelle, and J. P. Severinghaus (2012), Little Ice Age cold interval in West Antarctica: Evidence from borehole temperature at the West Antarctic Ice Sheet (WAIS) Divide, *Geophys. Res. Lett.*, *39*, L09710, doi:10.1029/2012GL051260.

1.   Introduction

1.1.   The Last 1000 Years

[2]   The Northern Hemisphere experienced a widespread cooling from about 1400 to 1850 C.E., often referred to as the Little Ice Age (hereafter LIA). The LIA was the latest of a series of centennial scale oscillations in the climate [*Wanner et al.*, 2011]. Understanding the cause of this type of event is key to our knowledge of the variability in the climate system, and to our ability to forecast future climate changes. The LIA cooling was associated with a time of lower solar irradiance and increased persistent volcanism [*Mann et al.*, 2009]. This forcing must have been amplified by natural feedbacks, because the magnitude of the forcing by itself is too small to explain the observed response. It is still unclear whether the Southern Hemisphere high latitudes had a temperature response synchronous to that of the Northern Hemisphere: changes in the solar forcing would call for hemispheric synchroneity, but evidence from the southward movement of the Inter-tropical Convergence Zone in the Pacific Ocean [*Sachs et al.*, 2009], and from changes in the ocean circulation [*Keigwin and Boyle*, 2000] argue for a delayed [*Goosse et al.*, 2004] or inverse response [*Broecker*, 2000].

1.2.   Site Description

[3]   We present here borehole temperature data from WAIS Divide (79°28′S, 112°05′W, 1766 m a.s.l.), situated near the flow divide at the center of West Antarctica. The relatively low elevation of West Antarctica allows marine air masses to penetrate into the continent interior, bringing with them heavy precipitation and warmer temperatures [*Nicolas and Bromwich*, 2011]. WAIS Divide has a mean annual air temperature of −28.5°C, and accumulation rate of 0.22 m_{ice}/yr, making it a good southern analog to the summit of Greenland (−29.5°C, 0.24 m_{ice}/yr [*Shuman et al.*, 2001]), thus a good candidate for inter-hemispheric comparisons. WAIS Divide is also strongly connected to the climate of the South Pacific [*Ding et al.*, 2011], and is sensitive to El-Niño Southern Oscillation [*Mayewski et al.*, 2009; *Fogt et al.*, 2011].

[4]   Borehole temperature measurements take advantage of the advection and diffusion of heat through the snow and ice. Both the thickness of the ice sheet and the high accumulation rate allow the climate signal to be better preserved at WAIS Divide than anywhere in central East Antarctica. We used a model of heat advection and diffusion in the ice to quantify this process, and an inversion scheme to reconstruct the surface temperature history from the borehole measurements.

2.   Method

2.1.   Sampling Method

[5]   The 300 m air-filled hole WDC05A (79°28′S, 112°05′W) was drilled in January 2005, and sampled both in January 2008 and January 2009 with a single thermistor (Omega 44033) connected to a precision multimeter (Fluke 8846A, 6 1/2 digits) using the 4-wire measurement method. The thermistor was calibrated at Scripps Institution of Oceanography against a secondary reference temperature standard, according to the Steinhart-Hart equation. The accuracy of the absolute temperature of this calibration is 0.1 K, and its relative uncertainty in the range of our borehole measurements is 0.0023 K. The inversion of borehole temperature measurements is not sensitive to the absolute temperature, but to the relative temperature difference between data points. Therefore, we are not as concerned about systematic biases in the whole profile as we are about errors that affect each data point, or each depth differently.

[1]Scripps Institution of Oceanography, University of California, San Diego, La Jolla, California, USA.

Corresponding author: A. J. Orsi, Scripps Institution of Oceanography, University of California, San Diego, 9500 Gilman Dr., La Jolla, CA 92037, USA. (aorsi@ucsd.edu)
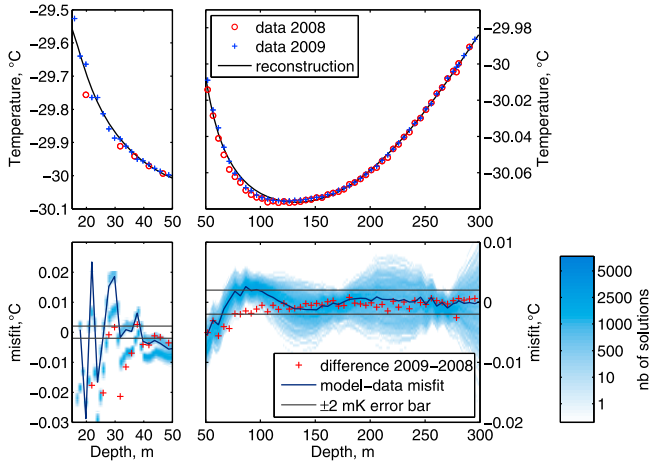
Figure 1. (top) WAIS Divide borehole temperature data, measured in a dry 300 m hole. There is no significant difference between the measurements made in 2008 and 2009. (bottom) Misfit between the best reconstruction and the data. In black is the stated 1-σ error in the data. The red symbols (+) show the difference between data measured in 2008 and 2009. The light blue shading represents the probability of each of the 6000 solutions generated to have the stated misfit with the data. All solutions fit the data reasonably well.

[6] In the field, the sensor was held stationary every 5 meters to equilibrate with the surrounding temperature for 20 min, and the resistance was integrated over 5 min. Logging was done both upwards and downwards, with 2 or 3 measurements at each depth. There is no significant difference between the profiles measured in 2009 vs 2008 below 30 m (Figure 1). The pooled standard deviation of all measurements, including both years, is 1.8 mK. This figure represents the reproducibility of the measurements, and may be taken as an estimate of the overall precision, which includes the noise from the instrument and local variability from air movement in the hole. The calibration is the leading source of uncertainty, and we consider the overall precision to be 2.3 mK.

2.2. Forward Model

[7] The forward firn and ice model is based on the 1 dimensional heat and ice flow equation, discretized in an explicit finite difference scheme, following *Alley and Koci* [1990]:

$$\rho c_p \frac{\partial T}{\partial t} = \frac{\partial}{\partial z}\left(k\frac{\partial T}{\partial z}\right) - \rho c_p w \frac{\partial T}{\partial z} + Q \qquad (1)$$

where ρ is the density of firn/ice, k the thermal conductivity, c_p the heat capacity, T the temperature, t the time, z the depth, w the downward velocity of the firn/ice, and Q the heat production term, taking into account ice deformation and firn compaction. WAIS Divide is near the ice flow divide, and the horizontal advection of mass and heat are both negligible.

[8] The density and accumulation rate are taken from onsite measurements [*Battle et al.*, 2011; *Banta et al.*, 2008]. The vertical velocity of the firn or ice w is determined using a constant strain rate, following *Cuffey et al.* [1994]. The heat capacity c_p, thermal conductivity k and heating term Q are all determined according to the classical equations

[*Cuffey and Paterson*, 2010, Chap. 9]. A detailed description of the model, and the uncertainties associated with each parameter is available in the auxiliary material.[1]

2.3. Inverse Model

[9] The diffusion process blurs the true temperature history, and this problem is classically underdetermined: there are an infinite number of possible temperature histories that would fit the data perfectly [*Clow*, 1992]. In addition, most of the parameters in Equation (1) depend on temperature, which makes the problem non-linear. Finding a solution requires us to make assumptions about what we consider to be a plausible solution, so that we can reduce the dimensionality of the problem. The details of the inverse method will therefore have an impact on the "best" solution found [*Shen et al.*, 1992].

[10] At least three approaches have been used to overcome this problem. A Monte Carlo scheme can be used to explore the range of possible solutions [e.g., *Dahl-Jensen et al.*, 1998]. Other types of data, like water isotopes, can be included as additional constraints on the temperature history [*Cuffey and Clow*, 1997]. A third approach is to linearize the problem, and find a solution by a generalized least-squares method [e.g., *MacAyeal et al.*, 1991; *Muto et al.*, 2011]. This method has the advantage of providing information about the unresolved dimensions of the problem. We chose here to use a generalized least-squares method, with the constraints highlighted below.

[11] Figure 2 shows the unavoidable smoothing of the record as we go back in time. In 1800 C.E., we can only reconstruct a non-uniform 220-year average temperature [*Clow*, 1992]. With this in mind, we do not try to specify high-frequency changes in past climate, but rather we focus on long-term changes. As a consequence, we will choose
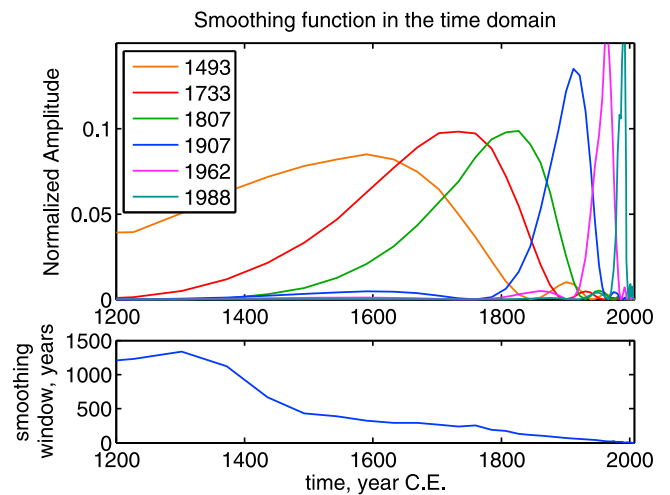
Figure 2. (top) Implied smoothing function for select times. (bottom) Smoothing window, calculated as the width of the smoothing function at half maximum. As we go back in time, the borehole temperature reconstruction effectively calculates the weighted average temperature over the time period given by the smoothing function. The high frequency variability of the climate is therefore blurred.
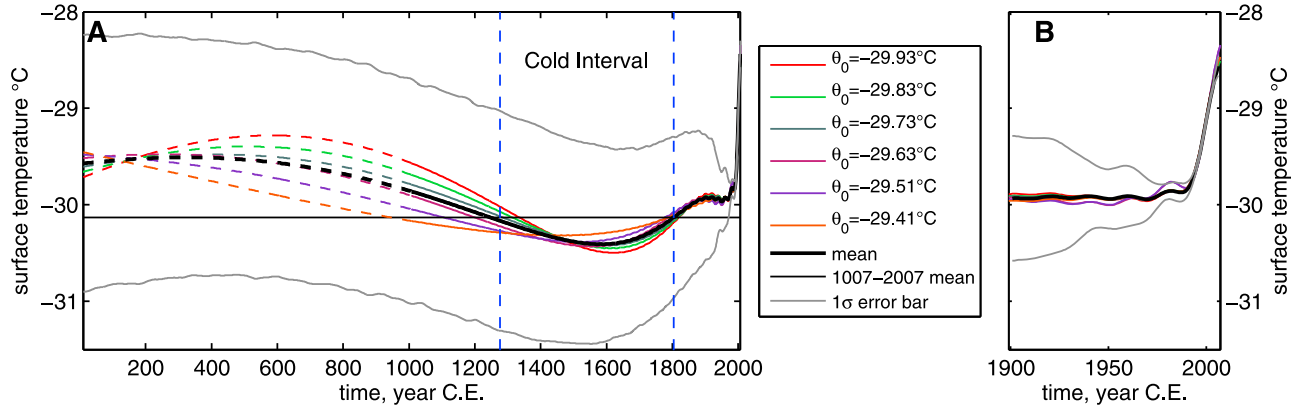
Figure 3. (a, b) Surface temperature reconstruction. Colored lines represent the optimal reconstruction for a range of initial conditions. Grey lines represent the 1 σ distribution of 6000 solutions (see section 2.4.1). The thick black line is the mean of all reconstructions, and was below the 1000 year average between 1300 and 1800 C.E. This reconstruction shows the smallest amount of change from a constant climate permitted by the data. Borehole temperature-based reconstructions lose resolution of higher frequencies going back in time; therefore, we cannot draw conclusions about the unusual character of the warming of the last 20 years.

among the infinite possibilities a solution with a small change in climate for a long timescale, rather than a short event of much larger amplitude. The net result is that all the extrema of temperature shown in this study are lower bounds of the actual climate history. It should also be noted that the method resolves high frequencies better as we get closer to the present: the reconstruction shows more details in the last 50 years (Figure 3b). For this reason, we caution that this study is not able to compare the warming of the last few decades to the longer-term context.

2.3.1. Linearization

[12] The forward model was linearized along an initial temperature history $\theta_0(t)$, which allowed us to use a least-squares regression to find the optimal solution [*Wunsch*, 1996, Chap. 3].

[13] The functional space of temperature history can be expressed as a linear combination of basis functions b_i: $\theta(t) = \theta_0(t) + \sum_i x_i b_i(t)$ where $\theta(t)$ is a history of temperature, t is the time, and $x(i)$ the coefficients of this linear combination. In vector notation, we can write:

$$\boldsymbol{\theta} = \boldsymbol{\theta_0} + \mathbf{Bx} \; with \; \mathbf{B} = [\mathbf{b_1 \, b_2 \, ... b_n}] \qquad (2)$$

We used a Fourier decomposition for $\mathbf{b_i}$, with periods between 4000 years (twice our window) and 20 years, with an amplitude of 1°C. Periods smaller than 20 years are quickly damped and do not contribute significantly to the solution. We also used a piecewise linear basis as an independent comparison. The influence of the choice of the basis functions is discussed in the auxiliary material.

[14] Each basis function $b_i(t)$ was run through the forward model to produce a temperature profile $y_i(z)$. We define $h_i(z) = y_i(z) - y_0(z)$, with y_0 the output of our initial guess $\theta_0(t)$. If the model is approximately linear, any temperature profile $y(z)$ can be expressed as a linear combination of the vectors $h_i(z)$. In vector notation: $\mathbf{y} = \mathbf{y_0} + \mathbf{Hx}$ *with* $\mathbf{H} = [\mathbf{h_1 \, h_2 \, ... \, h_n}]$. We want to find a history of temperature $\theta(t)$ that would fit our data $d(z)$, or the vector $\mathbf{d}$. This is equivalent to finding $\mathbf{x}$ so that

$$\mathbf{d} - \mathbf{y_0} = \mathbf{Hx} \qquad (3)$$

2.3.2. Least-Squares Regression

[15] Of the many solutions to equation (1), we are looking for the solution that satisfies the following assumptions:

[16] 1. The changes in the climate are as small as possible. Thus we chose $\theta_0(t)$ to be a constant temperature, and used the least-squares algorithm to minimize the temperature difference.

[17] 2. The lower frequencies are allowed a larger variance than the higher frequencies, reflecting preference for long-term climate variations. This assumption is implemented in the diagonal a-priori error covariance matrix of the model $\mathbf{P}$, whose elements are: $P_{i,i} = \sigma_x^2 \frac{f_i^{-2}}{\sum_i f_i^{-2}}$ with f_i the frequency of the sin/cos used in the basis functions b_i, and σ_x the a-priori root mean square error of the model parameters.

[18] 3. The amplitude of the climate changes is on the order of $\sigma_x = 0.5°C$, following the work of *Dahl-Jensen et al.* [1999] at Law Dome, where they found using a Monte Carlo scheme that the standard deviation of the reconstructed past temperature was around 0.3°C.

[19] The influence of the choice of the matrix P is discussed in the auxiliary material. The error in the data is represented by the diagonal matrix $\mathbf{R}$ whose elements are σ_d^2, with $\sigma_d = 0.002°C$, which reflects the precision of our measurements. The Least-squares theory shows that the optimum solution to (3) is:

$$\mathbf{x_1} = \mathbf{PH_1^T} \left(\mathbf{H_1 PH_1^T} + \mathbf{R} \right)^{-1} (\mathbf{d} - \mathbf{y_0}) \qquad (4)$$

The same linearization exercise can be performed around $\theta_1 = \theta_0 + \mathbf{Bx_1}$, with the output profile $\mathbf{y_1}$, creating a matrix $\mathbf{H_2}$. Subsequent solutions take the form [*El Akkraoui et al.*, 2008]:

$$\sum_{j=1}^{n} \mathbf{x_j} = \mathbf{PH_n^T} \left(\mathbf{H_n PH_n^T} + \mathbf{R} \right)^{-1} \left(\mathbf{d} - \mathbf{y_{n-1}} + \mathbf{H_n} \sum_{j=1}^{n-1} \mathbf{x_j} \right) \qquad (5)$$

The history of temperature is recovered using equation (2).
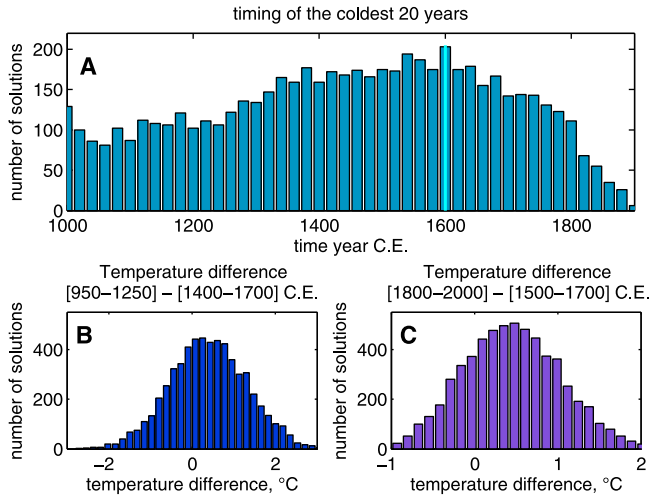
Figure 4. (a) Timing of the coldest 20 year interval using statistics made from 6000 solutions with various initial conditions (see text). Half of the solutions have a minimum between 1420 and 1760 C.E.. The most common minimum occurs in 1600 C.E. (b) Temperature difference between the average over the time period 950–1250 (Medieval Warm Period), and the average over 1400–1700 (Little Ice Age). The mean of this distribution is 0.39°C, and the standard deviation 0.93°C. A one sided student's t test performed on 6000 solutions confirms that the MWP was at least 0.33°C warmer than the LIA at WAIS Divide at the 99% confidence level. (c) Temperature difference between the average over the last 200 years, and the coldest period of 1500–1700 C.E. The mean of this distribution is 0.43°C, and the standard deviation 0.59°C.

2.4. Uncertainty Estimation

2.4.1. Uncertainty Associated With the Least-Squares Optimization

[20] The least-squares optimization provides a new estimate of the covariance of the uncertainty in the model parameters: $\hat{\mathbf{P}} = \mathbf{P} - \mathbf{PH_n^T}(\mathbf{H_n P H_n^T} + \mathbf{R})^{-1}\mathbf{H_n P}$. The largest eigenvectors of $\hat{\mathbf{P}}$ represent the dimensions least constrained by the data, which allows us to explore the statistics of the reconstruction. By choosing a stationary prior, we allow a lot of variability to be included in the uncertainty ensemble. In the distant past, all high frequencies are poorly determined. They do not figure in the optimal least-squares solution, but they are included in the uncertainty ensemble. Our uncertainty estimate is therefore very conservative.

[21] The 1-σ error on the reconstruction is given by the square root of the diagonal elements of $\mathbf{S} = \mathbf{B}\hat{\mathbf{P}}\mathbf{B^T}$, but this metric neglects the covariance between the temperature at a certain time, and the temperature a few years before or after.

[22] A series of solutions to (3) can be created using the eigenvalue decomposition of $\hat{\mathbf{P}} = \mathbf{UDU^T}$, where $\mathbf{U}$ is the matrix of eigenvectors, and $\mathbf{D}$ the diagonal matrix of the eigenvalues. A solution x_m takes the form:

$$\mathbf{x_m} = \mathbf{x} + \mathbf{U}\sqrt{\mathbf{D}}\,\mathbf{m} \qquad (6)$$

with **m** a vector of random numbers with zero mean and unit variance, **x** the optimum least-squares solution, and $\sqrt{\mathbf{D}}$ the

element by element square root of the diagonal matrix **D**. We used a series of $\mathbf{x_m}$ to explore the position and magnitude of extrema (Figure 4). Each one of these solutions was passed through the forward model, and the fit to the data is plotted as the shading in Figure 1. The fact that all models can fit the data within the stated error justifies the validity of the linearization around the optimal solution.

2.4.2. Uncertainty in the Timing of the Temperature Minimum

[23] We explored the smoothing created by both the physical diffusion of heat and our inversion technique by using the same linearization method, but taking piecewise linear functions for the $b_i(t)$. Each line of the resolution matrix $\mathbf{A} = \mathbf{PH^T}(\mathbf{HPH^T} + \mathbf{R})\mathbf{H}$ represents the weight given to the temperature at different times in the reconstructed temperature at the specific time corresponding to that line. Figure 2 shows a few examples of this smoothing function. We also explored the timing of the temperature minimum for a series of solutions, using equation (6), and the statistics are plotted in Figure 4. In addition, the thermal conductivity and accumulation rate have an impact on the timing of the extrema. Decreasing k by 10% results in a shift of the temperature minimum by 58 years. If the mean accumulation were 10% lower, the amplitude of the minima in the reconstruction would increase by 10%, and the temperature minimum would occur 38 years earlier (see the auxiliary material for details).

3. Results and Discussion

[24] The temperature measurements show a minimum at 125 m (Figure 1; $-0.2°C$ compared to the 30 m depth value), separating a deeper upward cooling trend from a more shallow upward warming. We interpret this minimum as direct evidence that there was a colder climate at some time in the past, a conclusion that is independent of the model and the inversion.

[25] The inversion-based reconstruction of snow surface temperature (Figure 3) shows a long term cooling trend from 1000 C.E. to a minimum in seventeenth century. The subsequent warming paused at the beginning of the twentieth century, and accelerated in the last ~20 years.

3.1. Seventeenth Century Minimum

[26] This temperature reconstruction shows a broad minimum circa 1600 C.E., the timing of which is not constrained very precisely by the data. We estimated the uncertainty in the timing using a distribution of 6000 solutions obtained using equation (6) (Figure 4a), and extracted meaningful information by comparing long time intervals. Half of the solutions have a minimum between 1420 and 1760 C.E. The temperature in the time period 1400–1800 was $0.52 \pm 0.28°C$ colder than the last 100-year average. We followed the nomenclature of *Mann et al.* [2009] to calculate the temperature difference between the period 950–1250 C.E. (often referred to as the Medieval Warm Period, MWP) and the period 1400–1700 C.E. (Figure 4b). The period 1400–1700 was on average $0.39 \pm 0.93°C$ colder than 950–1250 C.E. A one tailed student's t test shows that it was at least 0.33°C colder at the 99% confidence level. The coldest 200 years, 1500–1700 C.E., were at least 0.43°C colder than the period 1800–2000 C.E. at the 99% confidence level, with a mean of 0.43°C and standard deviation of 0.59°C
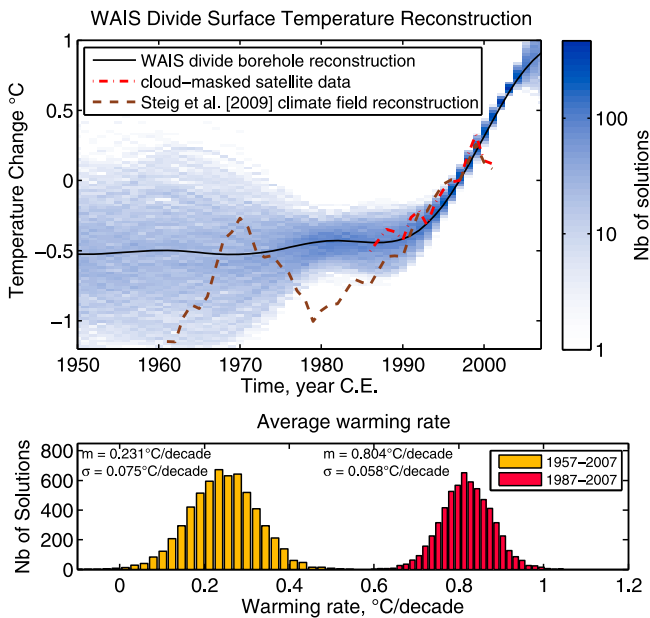
Figure 5. (top) Temperature reconstruction over the last 50 years. The shading shows the number of solutions with a specific temperature, based on 6000 solutions (see text). Temperature from cloud masked satellite data and climate field reconstruction [*Steig et al.*, 2009] are independent estimates of the temperature at WAIS-D, and are in good agreement with our reconstruction. (bottom) Histograms of the average warming rate over the periods 1957–2007 and 1987–2007, based on 6000 solutions to the borehole temperature profile. The warming trend has been intensifying.

(Figure 4c). Overall, from 1300 to 1800 C.E, the mean temperature was colder than the last 1000 year average.

[27] This reconstruction is consistent with the temperature estimate based on bubble number density in the WAIS Divide ice core. *Fegyveresi et al.* [2011] found that the temperature of WAIS Divide cooled by 1.7°C between 0 and 1700 C.E. Water isotopes from the same ice core also show a long term negative trend over the last 2000 years (E. Steig, personal communication, 2011).

[28] In other Antarctic ice cores, records of water isotopes ($\delta^{18}O$ and δD of H_2O) also support the idea of a long term cold interval centered around 1600 C.E. [*Bertler et al.*, 2011]. Talos Dome and Taylor Dome, in the Ross Sea Region of East Antarctica, have persistent negative isotopic values around 1600 C.E. [*Stenni et al.*, 2002]. Dome C has a weaker and longer negative excursion from 1400 to 1700 C.E. However, these records are often difficult to interpret in terms of temperature: changes in the elevation at the site and in the moisture source have dominant effects, and are challenging to constrain [*Masson et al.*, 2000]. In addition, other records have weak trends (South Pole [*Mosley-Thompson et al.*, 1993]), or slightly increasing trends (Siple Dome [*Mayewski et al.*, 2004]), raising the possibility of considerable spatial heterogeneity of the climate signal within Antarctica.

[29] In Southern South America, tree ring records have shown a pronounced summer cooling period between 1350

and 1700 C.E. [*Neukom et al.*, 2011], and a later cold event around 1850 C.E., which is consistent with our record.

[30] A similar borehole temperature record at GRIP, Greenland, shows two temperature minima in 1550 and 1850 C.E., with respective temperatures 0.34 and 0.49 K relative to the last 1000 year average (−31.82°C) [*Dahl-Jensen et al.*, 1998]. The summit of Greenland has a mean annual temperature and accumulation similar to that of WAIS Divide, and is a good candidate for inter-hemispheric comparison. Both sites are in the continental interior, and are thought to be representative of their respective regional climate [*Kobashi et al.*, 2010; *Steig et al.*, 2009]. The fact that WAIS Divide was colder than the last 1000 year average from 1300 to 1800 C.E. supports the idea that the Little Ice Age was not confined to the North Atlantic, and that a decrease in solar activity accompanied by persistent explosive volcanism was the cause of this event [*Miller et al.*, 2012]. The amplitude of the LIA cooling is half as much at WAIS Divide as it is at Greenland Summit, suggesting that feedbacks amplifying the radiative forcing may have been stronger in Greenland.

3.2. Recent Warming

[31] WAIS Divide has been warming by 0.23 ± 0.08°C per decade over the last 50 years. This warming rate has accelerated over the last 20 years to an average of 0.80 ± 0.06°C per decade (Figure 5).

[32] The Kominko-Slade weather station was fully operational in 2009 and 2010, and the measured annual average air temperature was −28.4°C in 2009, and −28.5°C in 2010, in good agreement with our reconstruction (Matthew Lazzara, AMRC, SSEC, UW-Madison).

[33] *Steig et al.* [2009] and *O'Donnell et al.* [2011] used weather station and satellite data to reconstruct the temperature history of Antarctica over 1957–2006. *Steig et al.* [2009] found an average warming rate of 0.17 ± 0.06°C for the West Antarctic Continent, and of 0.23 ± 0.09°C/decade at WAIS Divide, which is in good agreement with our results. *O'Donnell et al.* [2011] found weaker trends (0.10 ± 0.09°C/decade for West Antarctica) but also noticed a large increase in the trend at nearby Byrd station from 0.05 ± 0.13°C/decade over the period 1957–2006 to 0.20 ± 0.36°C/decade for 1982–2006. These data sets also show that the warming is concentrated in the winter and spring seasons. It is associated with a decrease in sea ice in the Amundsen and Bellingshausen Seas, and an increase in sea ice in the Ross Sea [*Parkinson*, 2002]. It has been attributed to an increase in warm advection through the Amundsen Sea, associated with a strong teleconnection with the central tropical Pacific Ocean [*Schneider et al.*, 2012; *Ding et al.*, 2011].

[34] The inversion of borehole temperature does not allow us to comment on whether this warming rate is unprecedented, because of the loss of temporal resolution with time (Figure 2).

4.   Conclusion

[35] WAIS Divide was colder than the last 1000-year average from 1300 to 1800 C.E. This trend is broadly synchronous with the large-scale cooling of 1400–1700 C.E. in the Northern Hemisphere, although the details of these records are not in phase. These findings support the

hypothesis that solar minima, associated with persistent volcanism, can noticeably cool the planet, but the feedbacks amplifying the radiative forcing may operate differently in each hemisphere.

[36] This record also confirms the work of *Steig et al.* [2009], showing that WAIS Divide has been warming by 0.23 ± 0.08 °C per decade over 1957–2007 C.E. This warming trend has accelerated to 0.8 ± 0.06 °C per decade over the last 20 years (1987–2007). It is thought to be associated with a stronger teleconnection with the central tropical Pacific, which induces increased warm advection into the continental interior in winter and spring [*Ding et al.*, 2011], and not with the increase in polar westerlies due to the ozone hole. It is unclear whether this warming is unprecedented, or whether it fits within the natural variability of West Antarctica. Other data that do not have the same type of limitation, such as water isotopes or noble gases from ice cores [*Kobashi et al.*, 2010], will provide additional constraints on this issue.

[37] Much remains to be understood about the variability in the West Antarctic climate. Records like this one provide important boundary conditions for climate models in a part of the world with notoriously sparse data coverage.

[39] The Editor thanks Kurt Cuffey and two anonymous reviewers for assisting with the evaluation of this paper.

References

Alley, R. B., and B. R. Koci (1990), Recent warming in central Greenland?, *Ann. Glaciol.*, 14, 6–8.

Banta, J., J. McConnell, M. Frey, R. Bales, and K. Taylor (2008), Spatial and temporal variability in snow accumulation at the West Antarctic Ice Sheet Divide over recent centuries, *J. Geophys. Res.*, 113, D23102, doi:10.1029/2008JD010235.

Battle, M. O., J. P. Severinghaus, E. D. Sofen, D. Plotkin, A. J. Orsi, M. Aydin, S. A. Montzka, T. Sowers, and P. P. Tans (2011), Controls on the movement and composition of firn air at the West Antarctic Ice Sheet Divide, *Atmos. Chem. Phys.*, 11(21), 11,007–11,021, doi:10.5194/acp-11-11007-2011.

Bertler, N., P. Mayewski, and L. Carter (2011), Cold conditions in Antarctica during the Little Ice Age—Implications for abrupt climate change mechanisms, *Earth Planet. Sci. Lett.*, 308(1–2), 41–51, doi:10.1016/j.epsl.2011.05.021.

Broecker, W. S. (2000), Was a change in thermohaline circulation responsible for the Little Ice Age?, *Proc. Natl. Acad. Sci. U. S. A.*, 97(4), 1339–1342, doi:10.1073/pnas.97.4.1339.

Clow, G. (1992), The extent of temporal smearing in surface-temperature histories derived from borehole temperature measurements, *Palaeogeogr. Palaeoclimatol. Palaeoecol.*, 98(2–4), 81–86, doi:10.1016/0031-0182(92)90189-C.

Cuffey, K., and G. Clow (1997), Temperature, accumulation, and ice sheet elevation in central Greenland through the last deglacial transition, *J. Geophys. Res.*, 102(C12), 26,383–26,396, doi:10.1029/96JC03981.

Cuffey, K., and W. Paterson (2010), *The Physics of Glaciers*, Academic, Amsterdam.

Cuffey, K., R. Alley, P. Grootes, J. Bolzan, and S. Anandakrishnan (1994), Calibration of the δ^{18}O isotopic paleothermometer for central Greenland, using borehole temperatures, *J. Glaciol.*, 40(135), 341–349.

Dahl-Jensen, D., K. Mosegaard, N. Gundestrup, G. D. Clow, S. J. Johnsen, A. W. Hansen, and N. Balling (1998), Past temperatures directly from the Greenland ice sheet, *Science*, 282(5387), 268–271, doi:10.1126/science.282.5387.268.

Dahl-Jensen, D., V. I. Morgan, and A. Elcheikh (1999), Monte carlo inverse modelling of the Law Dome (Antarctica) temperature profile, *Ann. Glaciol.*, 29(1), 145–150, doi:10.3189/172756499781821102.

Ding, Q., E. J. Steig, D. S. Battisti, and M. Küttel (2011), Winter warming in West Antarctica caused by central tropical Pacific warming, *Nat. Geosci.*, 4, 398–403, doi:10.1038/ngeo1129.

El Akkraoui, A., P. Gauthier, S. Pellerin, and S. Buis (2008), Intercomparison of the primal and dual formulations of variational data assimilation, *Q. J. R. Meteorol. Soc.*, 134(633), 1015–1025, doi:10.1002/qj.257.

Fegyveresi, J., R. Alley, M. Spencer, J. Fitzpatrick, E. Steig, J. White, J. McConnell, and K. Taylor (2011), Late-Holocene climate evolution at the WAIS Divide site, West Antarctica: Bubble number-density estimates, *J. Glaciol.*, 57(204), 629–638, doi:10.3189/002214311797409677.

Fogt, R., D. Bromwich, and K. Hines (2011), Understanding the SAM influence on the South Pacific ENSO teleconnection, *Clim. Dyn.*, 36, 1555–1576, doi:10.1007/s00382-010-0905-0.

Goosse, H., V. Masson-Delmotte, H. Renssen, M. Delmotte, T. Fichefet, V. Morgan, T. van Ommen, B. K. Khim, and B. Stenni (2004), A late medieval warm period in the Southern Ocean as a delayed response to external forcing?, *Geophys. Res. Lett.*, 31, L06203, doi:10.1029/2003GL019140.

Keigwin, L. D., and E. A. Boyle (2000), Detecting Holocene changes in thermohaline circulation, *Proc. Natl. Acad. Sci. U. S. A.*, 97(4), 1343–1346, doi:10.1073/pnas.97.4.1343.

Kobashi, T., J. P. Severinghaus, J.-M. Barnola, K. Kawamura, T. Carter, and T. Nakagawa (2010), Persistent multi-decadal Greenland temperature fluctuation through the last millennium, *Clim. Change*, 100(3–4), 733–756, doi:10.1007/s10584-009-9689-9.

MacAyeal, D., J. Firestone, and E. Waddington (1991), Paleothermometry by control methods, *J. Glaciol.*, 37(127), 326–338.

Mann, M. E., Z. Zhang, S. Rutherford, R. S. Bradley, M. K. Hughes, D. Shindell, C. Ammann, G. Faluvegi, and F. Ni (2009), Global signatures and dynamical origins of the Little Ice Age and Medieval Climate Anomaly, *Science*, 326(5957), 1256–1260, doi:10.1126/science.1177303.

Masson, V., et al. (2000), Holocene climate variability in Antarctica based on 11 ice-core isotopic records, *Quat. Res.*, 54(3), 348–358, doi:10.1006/qres.2000.2172.

Mayewski, P. A., et al. (2004), A 700 year record of Southern Hemisphere extratropical climate variability, *Ann. Glaciol.*, 39(1), 127–132, doi:10.3189/172756404781814249.

Mayewski, P., et al. (2009), State of the Antarctic and Southern Ocean climate system, *Rev. Geophys.*, 47, RG1003, doi:10.1029/2007RG000231.

Miller, G. H., et al. (2012), Abrupt onset of the Little Ice Age triggered by volcanism and sustained by sea-ice/ocean feedbacks, *Geophys. Res. Lett.*, 39, L02708, doi:10.1029/2011GL050168.

Mosley-Thompson, E., L. Thompson, J. Dai, M. Davis, and P. Lin (1993), Climate of the last 500 years: High resolution ice core records, *Quat. Sci. Rev.*, 12(6), 419–430, doi:10.1016/S0277-3791(05)80006-X.

Muto, A., T. A. Scambos, K. Steffen, A. G. Slater, and G. D. Clow (2011), Recent surface temperature trends in the interior of East Antarctica from borehole firn temperature measurements and geophysical inverse methods, *Geophys. Res. Lett.*, 38, L15502, doi:10.1029/2011GL048086.

Neukom, R., et al. (2011), Multiproxy summer and winter surface air temperature field reconstructions for southern South America covering the past centuries, *Clim. Dyn.*, 37(1–2), 35–51, doi:10.1007/s00382-010-0793-3.

Nicolas, J., and D. Bromwich (2011), Climate of West Antarctica and influence of marine air intrusions, *J. Clim.*, 24(1), 49–67, doi:10.1175/2010JCLI3522.1.

O'Donnell, R., N. Lewis, S. McIntyre, and J. Condon (2011), Improved methods for PCA-based reconstructions: Case study using the Antarctic temperature reconstruction, *J. Clim.*, 24, 2099–2115, doi:10.1175/2010JCLI3656.1.

Parkinson, C. (2002), Trends in the length of the Southern Ocean sea-ice season, 1979–99, *Ann. Glaciol.*, 34(1), 435–440, doi:10.3189/172756402781817482.

Sachs, J., D. Sachse, R. Smittenberg, Z. Zhang, D. Battisti, and S. Golubic (2009), Southward movement of the Pacific intertropical convergence zone AD 1400–1850, *Nat. Geosci.*, 2(7), 519–525, doi:10.1038/ngeo554.

Schneider, D. P., C. Deser, and Y. Okumura (2012), An assessment and interpretation of the observed warming of West Antarctica in the austral spring, *Clim. Dyn.*, 38, 323–347, doi:10.1007/s00382-010-0985-x.

Shen, P., K. Wang, H. Beltrami, and J. Mareschal (1992), A comparative study of inverse methods for estimating climatic history from borehole temperature data, *Palaeogeogr. Palaeoclimatol. Palaeoecol.*, 98(2–4), 113–127, doi:10.1016/0031-0182(92)90192-8.

Shuman, C., K. Steffen, J. Box, and C. Stearns (2001), A dozen years of temperature observations at the Summit: Central Greenland automatic weather stations 1987–99, *J. Appl. Meteorol. Climatol.*, 40, 741–752, doi:10.1175/1520-0450(2001)040<0741:ADYOTO>2.0.CO;2.

Steig, E. J., D. P. Schneider, S. D. Rutherford, M. E. Mann, J. C. Comiso, and D. T. Shindell (2009), Warming of the Antarctic ice-sheet surface since the 1957 International Geophysical Year, *Nature*, 457, 459–462, doi:10.1038/nature07669.

Stenni, B., M. Proposito, R. Gragnani, O. Flora, J. Jouzel, S. Falourd, and M. Frezzotti (2002), Eight centuries of volcanic signal and climate change at Talos Dome (East Antarctica), *J. Geophys. Res.*, *107*(D9), 4076, doi:10.1029/2000JD000317.

Wanner, H., O. Solomina, M. Grosjean, S. Ritz, and M. Jetel (2011), Structure and origin of Holocene cold events, *Quat. Sci. Rev.*, *30*, 21–22, doi:10.1016/j.quascirev.2011.07.010

Wunsch, C. (1996), *The Ocean Circulation Inverse Problem*, Cambridge Univ. Press, Cambridge, U. K., doi:10.1017/CBO9780511629570.